Check for updates

How to cite: *Angew. Chem. Int. Ed.* **2024**, *63*, e202400101
doi.org/10.1002/anie.202400101

Photocatalysis Hot Paper

Triazine Frameworks for the Photocatalytic Selective Oxidation of Toluene

Sizhe Li, Niklas Huber, Wei Huang, Wenxin Wei, Katharina Landfester, Calum T. J. Ferguson,* Yan Zhao,* and Kai A. I. Zhang*[+]

Abstract: Investigations into the selective oxidation of inert sp^3 C–H bonds using polymer photocatalysts under mild conditions have been limited. Additionally, the structure-activity relationship of photocatalysts often remains insufficiently explored. Here, a series of thiophene-based covalent triazine frameworks (CTFs) are used for the efficient and selective oxidation of hydrocarbons to aldehydes or ketones under ambient aerobic conditions. Spectroscopic methods conducted in situ and density functional theory (DFT) calculations revealed that the sulfur atoms within the thiophene units play a pivotal role as oxidation sites due to the generation of photogenerated holes. The effect of photogenerated holes on photocatalytic toluene oxidation was investigated by varying the length of the spacer in a CTF donor-acceptor based photocatalyst. Furthermore, the manipulation of reactive oxygen species was employed to enhance selectivity by weakening the peroxidative capacity. As an illustrative example, this study successfully demonstrated the synthesis of a precursor of the neurological drug AMG-579 using a photocatalytic protocol.

Introduction

The selective oxidation of hydrocarbons to aldehydes or ketones is crucial in organic synthesis and the chemical industry.[1] Traditional methods involve the use of catalytic metals or corrosive oxidants at high temperatures and pressures, which are expensive and pose environmental challenges.[2] The heterogeneous photocatalytic activation of C–H bonds with molecular oxygen is a promising alternative that uses abundant and clean oxygen as the terminal oxidant and solar energy as the driving force.[3] However, the efficient photocatalytic aerobic oxidation of hydrocarbons under ambient conditions is challenging because of the high chemical stability of sp^3 C–H bonds.[4] Current photocatalytic systems have limitations, such as the use of high-energy ultraviolet light and low charge separation efficiency, which limits their practical application.[5] To overcome these limitations, novel, environmentally friendly photocatalytic systems are needed for the efficient oxidative functionalization of hydrocarbons.

Photocatalytic oxidation of saturated C–H bonds has recently advanced rapidly.[6] To further enhance catalyst activity and selectivity, a comprehensive understanding of the underlying mechanisms is critical, particularly for preventing the over-oxidation of substrates.[7] Photogenerated holes play a vital role in the oxidation of hydrocarbons to alkyl radicals, which is a rate-limiting step because of the inertness of the sp^3 C–H bonds. Reactive oxygen species (ROS) then react with alkyl radicals to generate alcohol and carbonyl compounds. However, if the reaction medium contains excess strong oxidants such as hydroxyl radicals, further oxidation of the target products may occur, leading to unselective mineralization into CO_2 and water.[8] Therefore, the density of photogenerated holes and the type of reactive oxygen species are critical factors that significantly influence the efficiency and selectivity of the reaction.

Organic polymers have gained attention as metal-free and structurally robust materials for visible-light-induced organic syntheses.[9] Several strategies have been employed to enhance photocatalytic performance, including the use of tailored monomers,[10] elemental doping,[11] morphologically controlled synthesis,[12] and structural optimization.[13] However, the role of photogenerated holes at the oxidation sites has received little attention despite its potential to improve performance and selectivity. Photocatalytic polymers offer a flexible material platform with tunable properties. Despite their appeal, achieving the efficient aerobic oxidation of inert hydrocarbons with visible light and oxygen at ambient temperature and pressure using pure organic heterogeneous photocatalysts remains a challenge.

Covalent triazine frameworks (CTFs) are nitrogen-rich conjugated polymers that have been studied for solar energy conversion.[14] In this study, thiophene-based CTFs with

[*] S. Li, W. Wei, Prof. Y. Zhao, Prof. K. A. I. Zhang[+]
Department of Materials Science, Fudan University
200433 Shanghai, P. R. China
E-mail: weiwenxin@fudan.edu.cn
zhaoy@fudan.edu.cn

N. Huber, W. Huang, Prof. K. Landfester, Dr. C. T. J. Ferguson, Prof. K. A. I. Zhang[+]
Max Planck Institute for Polymer Research
55128 Mainz, Germany
E-mail: ferguson@mpip-mainz.mpg.de

[+] this author passed away during the preparation of this manuscript.

© 2024 The Authors. Angewandte Chemie International Edition published by Wiley-VCH GmbH. This is an open access article under the terms of the Creative Commons Attribution License, which permits use, distribution and reproduction in any medium, provided the original work is properly cited.

© 2024 The Authors. Angewandte Chemie International Edition published by Wiley-VCH GmbH

different spacer lengths were investigated as visible-light photocatalysts for the mild and selective aerobic oxidation of inert hydrocarbons under ambient conditions. Spectroscopic methods such as in situ X-ray photoelectron spectroscopy (XPS) and transient time-dependent density functional theory (TD-DFT) calculations were used to determine the major oxidation sites. In particular, optical pump THz-probe (OPTP) spectroscopy and femtosecond transient absorption (fs-TA) spectroscopy were used to study the photogenerated charge-carrier dynamics, thereby deepening our understanding of photogenerated hole production at the active oxidation sites. Kinetic studies of the photocatalytic oxidation of toluene to benzaldehyde were performed to determine the optimal spacer length. In situ diffuse reflectance infrared Fourier transform spectroscopy (DRIFTS) and electron spin resonance (ESR) techniques were employed to monitor the formation of intermediate products and reactive species, thereby providing valuable insights into the intricacies of the reaction mechanism.

Results and Discussion

A series of CTFs were synthesized through superacid-catalyzed polymerization in the solid phase to investigate the effect of the spacer length on the charge transfer and photocatalytic properties. The resulting CTFs are denoted as CTF-Th-x ($x=0,1,2$ according to the number of phenylene units between the thiophene donor and triazine acceptor units) (Figure 1a). Synthetic procedures details are provided in Supporting Information. The scanning electron microscopy and transmission electron microscopy images of

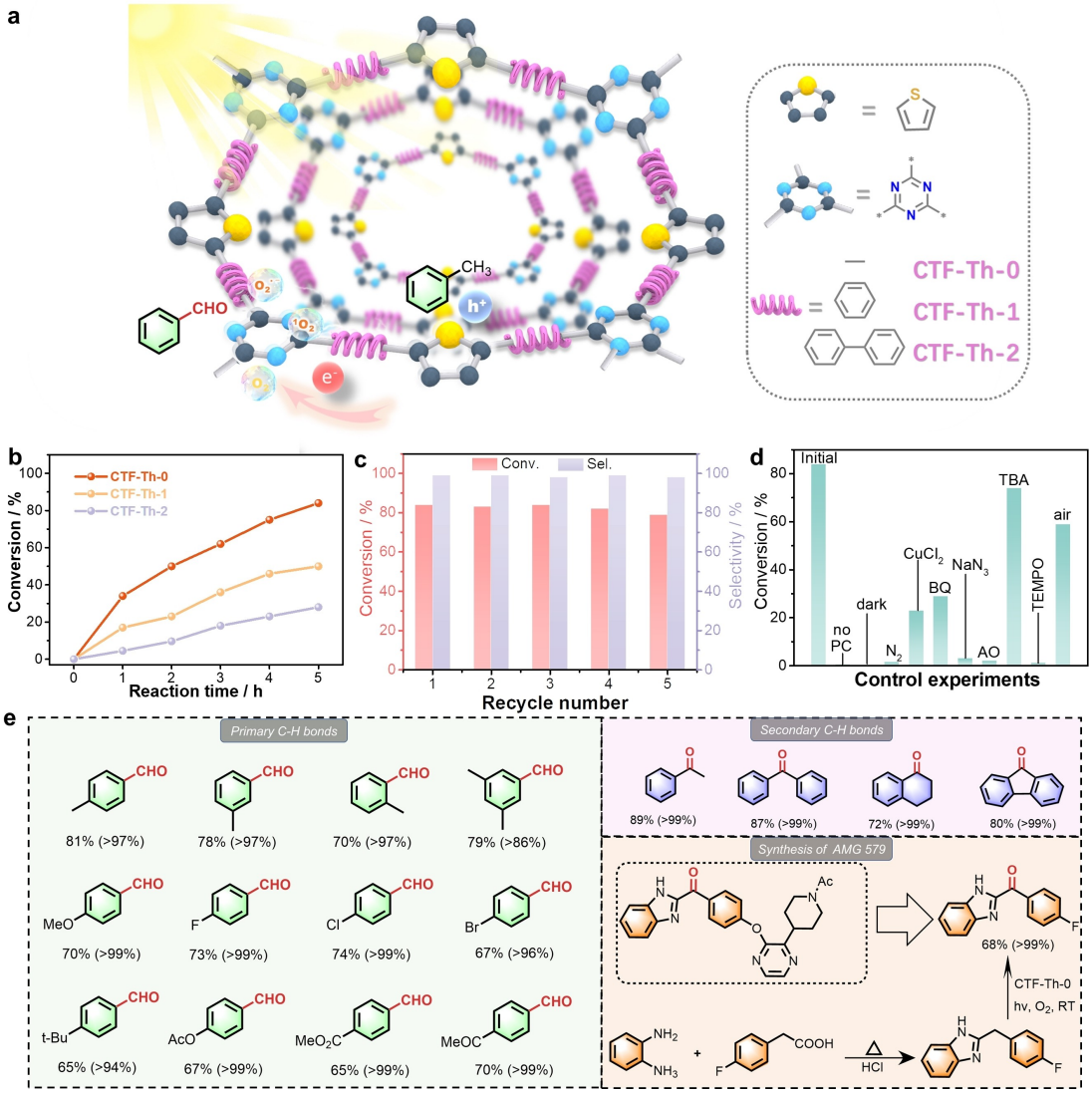

Figure 1. Preparation of CTFs and their photocatalytic performance. (a) Schematic illustration of the molecular engineering strategy of CTFs for the photocatalytic selective oxidation of toluene. (b) Efficiency comparison of the photocatalytic selective oxidation of toluene over different CTFs. (c) Catalytic durability of CTF-Th-0. (d) Control experiments. (e) Substrate scope for the visible-light-induced aerobic oxidation of C–H bonds in hydrocarbons.

© 2024 The Authors. Angewandte Chemie International Edition published by Wiley-VCH GmbH

15213773, 2024, 18, Downloaded from https://onlinelibrary.wiley.com/doi/10.1002/anie.202400101 by MPI 355 Polymer Research, Wiley Online Library on [24/04/2024]. See the Terms and Conditions (https://onlinelibrary.wiley.com/terms-and-conditions) on Wiley Online Library for rules of use; OA articles are governed by the applicable Creative Commons License

the CTF samples show hollow structures with diameters of approximately 300 nm. The energy-dispersive X-ray spectroscopy (EDX) mapping images confirmed that the elements C, N, and S were evenly distributed throughout the CTFs (Figure S5). The Fourier transform infrared (FT-IR) spectra (Figure S6) show two intense characteristic peaks from the triazine units at approximately 1500 and 1360 cm^{-1} in all the CTFs, indicating the successful formation of triazine frameworks. The absence of terminal nitrile groups suggests a high degree of polymerization. The solid-state ^{13}C cross-polarization magic-angle spinning (CP-MAS) NMR spectra of these CTFs revealed a distinctive peak. Specifically, a single sharp peak was observed at 167.3 ppm, attributable to the sp^2 carbon in the triazine unit. Additionally, for CTF-Th-0, peaks were observed at 170.4 ppm, for CTF-Th-1, peaks at 171.4 ppm, and for CTF-Th-2, peaks at 172.4 ppm, respectively, indicating the presence of the thiophene ring (Figure S7). The nitrogen sorption experiments measured at 77 K showed Brunauer–Emmett–Teller (BET) surface areas of 48, 38, and 68 $m^2 g^{-1}$ for the various CTFs (Figure S8). This low surface area is probably due to the method of preparation of the CTFs, where the CTFs lacked long-range ordered networks, as confirmed by powder X-ray diffraction (PXRD) (Figure S9) and were amorphous. Thermogravimetric analysis (TGA) indicated that the CTFs are thermally stable up to approximately 450 °C without significant weight loss (Figure S10). Interestingly, the stability of the CTFs seemed to be linked to the amount of phenyl units included in the CTF structure.

The optoelectronic properties of the CTFs were analyzed using solid-state UV/Vis diffuse reflection (DR) measurements. The visible-light absorption behavior of all the CTFs were similar, with absorption occurring from 550 nm to shorter wavelengths. A slight increase in the absorption onset wavelength from CTF-Th-0 to CTF-Th-2 occurred (Figure S11), resulting in a gradual decrease in the band gap from 2.47 eV for CTF-Th-0 to 2.40 eV for CTF-Th-1 and 2.37 eV for CTF-Th-2, as observed from the Kubelka–Munk transformed reflectance spectra (Figure S12). The yellow color of all the powders was consistent with these observations (Figure S13). To evaluate the energy levels of the CTFs, valence band X-ray photoelectron spectroscopy (VB-XPS) was performed.[15] The VB edge of CTF-Th-0, CTF-Th-1 and CTF-Th-2 was at 1.56 eV, 1.26 eV and 1.01 eV respectively, as shown in Figure S14. Therefore, using the VB value from the band gap energy, the potential of the conduction band (CB) was calculated to be −0.96 eV for CTF-Th-0, −1.17 eV for CTF-Th-1 and −1.39 eV for CTF-Th-2. The CTF band structures displayed in Figure S15 are consistent with the theoretical values calculated from the model compounds (Figure S16). The CB of the CTFs was sufficiently negative to reduce O_2, and the VB of the CTFs was inadequate to oxidize H_2O or OH groups to $^{\bullet}OH$ radicals. Additionally, DFT analysis revealed that small amounts of cyanides from the unpolymerized monomers could lower the highest occupied molecular (HOMO) and enhance the oxidative power of the CTFs (Figure S17).

Benzaldehyde is a commonly used aromatic aldehyde in various industries, and its production by conventional methods faces selectivity and turnover challenges.[16] We investigated the photocatalytic activity of the CTFs for the selective oxidation of toluene to benzaldehyde under visible-light irradiation using molecular oxygen as the terminal oxidant. Nitromethane was selected as the solvent, and the reactions were sampled at different times (1 to 5 h) and analyzed by gas chromatography-mass spectrometry (Figure S18). CTF-Th-0 showed the highest photocatalytic efficiency, with a conversion of 84 %, followed by CTF-Th-1 (47 %) and CTF-Th-2 (28 %) (Figure 1b). The TOF of CTF-Th-0 was estimated to be 2.2 $mmol\,g^{-1}\,h^{-1}$, outperforming the reported state-of-the-art catalysts (Table S1). By doubling the reaction time, the reaction was completed with 99 % conversion and 99 % selectivity (Figure S19). The conversion and selectivity of the reaction were highly dependent on the solvent choice, and a solvent-free experiment achieved a conversion of 1.02 %, a selectivity of > 99 %, and a TOF of 0.60 $mmol\,g^{-1}\,h^{-1}$ in 24 h of reaction time (Figure S20), pointing toward a potential green and scaled-up application without wasteful solvent consumption. Recycling experiments were conducted using sample CTF-Th-0 to assess the reusability and stability of the CTFs as a photocatalyst. CTF-Th-0 did not demonstrate any significant conversion rate or selectivity decrease after being used for five consecutive cycles (Figure 1c). Furthermore, the UV/Vis and FT-IR spectra of CTF-Th-0 after the recycling experiments exhibited minimal changes, indicating that the catalyst retained its chemical integrity throughout the process (Figure S21a and S21b). These findings confirmed the high stability and reusability of CTF-Th-0, making it an excellent candidate for practical photocatalytic applications.

Inspired by the high photocatalytic reactivity of CTF-Th-0 in the selective oxidation of toluene, we investigated the scope of this reaction (Figure 1e). The generality of this catalytic scheme was demonstrated through the conversion of substances with different substituents. As shown in Figure 1, o-, m-, and p-substituted toluene were readily oxidized to the corresponding aldehydes. Notably, the substituent did not change the selectivity but significantly affected the conversion rate. In addition, compared to m- and p-substituted toluene, o-substituted toluene had lower conversions owing to their increased steric hindrance. A series of p-substituted halogen compounds revealed that higher conversions were achieved with more electron-withdrawing substituents. These observations clearly indicate that both the electronic and steric effects of the substituents significantly affect the final photocatalytic efficiency. In addition to primary C–H bonds, secondary C–H bonds can also be effectively oxidized to the corresponding ketones with good conversion and selectivity. Cyclohexene was oxidized to cyclohexanone with 10 % conversion and > 99 % selectivity. This approach was also applicable to heteroatom-containing substrates, demonstrating moderate conversions but with high selectivity, giving this photocatalytic protocol potential applications in the preparation of pharmaceutically relevant intermediates. As a proof of concept, a nitrogen-containing heterocyclic ketone, an intermediate of the neurological drug AMG 579, was synthesized via a facile two-step route from a commercially available precur-

© 2024 The Authors. Angewandte Chemie International Edition published by Wiley-VCH GmbH

15213773, 2024, 18, Downloaded from https://onlinelibrary.wiley.com/doi/10.1002/anie.202400101 by MPI 355 Polymer Research, Wiley Online Library on [24/04/2024]. See the Terms and Conditions (https://onlinelibrary.wiley.com/terms-and-conditions) on Wiley Online Library for rules of use; OA articles are governed by the applicable Creative Commons License

sor. Compared to previously conducted syntheses, the visible-light-driven selective oxidation approach offers an economical and green pathway to obtain value-added products.

To gain a deeper understanding of the reaction mechanism involved in the selective photocatalytic oxidation of toluene using CTF-Th-0, we performed a series of control experiments (Figure 1d). The negligible product formation in the absence of a photocatalyst and light confirmed the photocatalytic nature of the process, while the almost terminated oxidative transformation of toluene under a N_2 atmosphere confirmed the essential role of oxygen in the reaction mechanism. The addition of $CuCl_2$ and benzoquinone (BQ) an as electron scavenger and superoxide radical ($O_2^{\bullet-}$) scavenger, respectively, resulted in a significant decrease in the conversion rate, highlighting the importance of these reactive intermediates in the reaction pathway. When NaN_3 was added as a $^1O_2$ scavenger, the conversion rate was only 2%, confirming the role of singlet oxygen ($^1O_2$) in the process. The addition of ammonia oxalate (AO) as a hole scavenger inhibited this reaction, indicating that photogenerated holes play a crucial role in toluene oxidation. The negligible effect of tert-butyl alcohol (TBA), a hydroxyl radical scavenger ($^\bullet$OH), on toluene conversion can be attributed to the high reactivity and non-selectivity of hydroxyl radicals in organic reactions, making a reaction pathway via hydroxyl radicals unlikely. Quenching of the reaction by (2,2,6,6-tetramethylpiperidin-1-yl)oxyl (TEMPO) suggested a radical mechanism. Furthermore, carrying out the reaction in air resulted in a reduction in catalytic activity, but the reaction still demonstrated a 56% conversion and >99% selectivity after 5 h of visible-light irradiation.

In situ diffuse reflectance infrared Fourier transform spectroscopy (DRIFTS) was used to detect the adsorbed species and intermediates formed on the surface of CTF-Th-0 during the selective photocatalytic oxidation of toluene. The process was monitored under dark (0–30 min), as shown in Figure 2a. Initially, bands ascribed to the benzene ring (3029 cm^{-1}) and methyl group (2933 cm^{-1}) of toluene were observed without light irradiation (0–30 min), indicating that toluene was adsorbed and activated on the surface. Upon light irradiation (Figure 2b), the intensities of the toluene vibrations decreased, and the newly emerged IR peaks in the range of 800–900 cm^{-1} due to the characteristic stretching of O–O bonds provided strong evidence of the formation of alkyl peroxy radicals, which have been identified as key intermediates. Notably, an absorption peak was detected at 1620 cm^{-1}, which indicated the formation of benzaldehyde. These results suggest that toluene was adsorbed on the CTFs, converted to an alkyl peroxy radical intermediate, and then further decomposed to obtain the final product, benzaldehyde. ESR experiments were conducted to identify the active species generated during the photocatalytic reaction. The observed decrease in the TEMPO signal over time, caused by its oxidation to $TEMPO^+$ via h^+, provided evidence of the formation of h^+ during the reaction (Figure 2c). Under the same experimental conditions, CTF-Th-0 exhibited the most significant reduction in signal intensity compared to those of the other CTFs, indicating that CTF-Th-0 exhibited the highest degree of photogenerated hole involvement in the reaction (Fig-

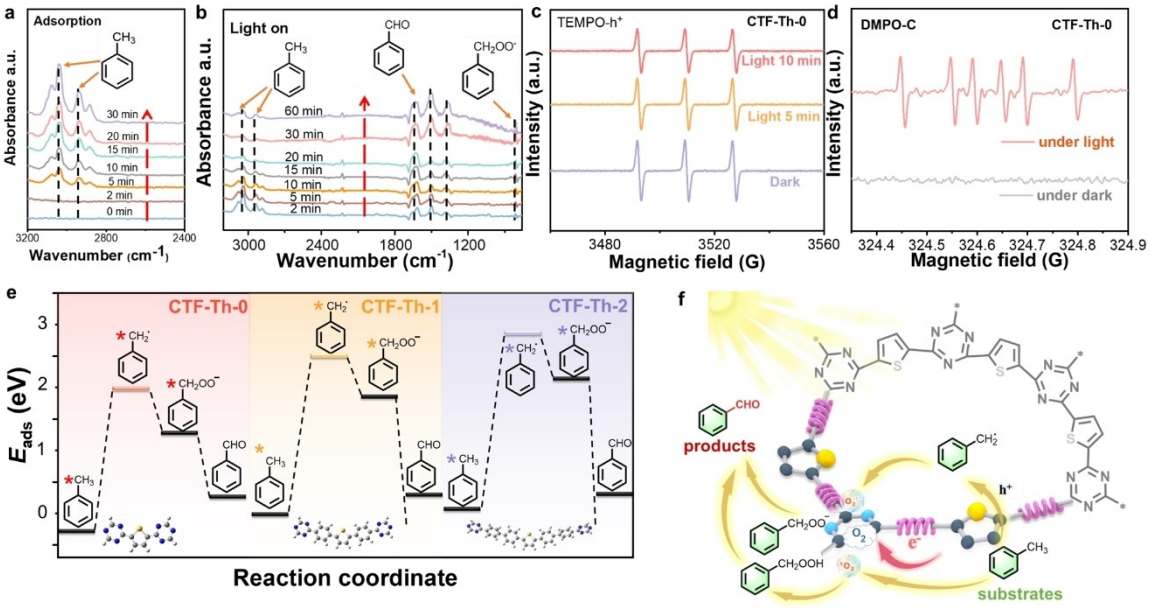

Figure 2. Mechanistic studies on the photocatalytic selective oxidation of toluene. (a), (b) In situ DRIFT spectra of the adsorption stage before the reaction and during the reaction process. (c) ESR spectra of holes (TEMPO-h^+) in an acetonitrile dispersion of CTF-Th-0 in the dark, with 5 min of irradiation, and with 10 min of irradiation. (d) In situ ESR spectra of CTF-Th-0, reaction conditions: 0.1 mmol of toluene, 5 mg of catalyst, and equivalent DMPO trapping agent were dispersed in 2 mL of nitromethane, bubbled under O_2 for 2 min, and irradiated at $\lambda > 460$ nm at room temperature. (e) DFT calculations for the effects of different CTFs on toluene adsorption (E_{ads}) and C(sp^3)–H bond dissociation. (f) Proposed mechanism of the photocatalytic oxidation of toluene toward benzaldehyde.

© 2024 The Authors. Angewandte Chemie International Edition published by Wiley-VCH GmbH

15213773, 2024, 18, Downloaded from https://onlinelibrary.wiley.com/doi/10.1002/anie.202400101 by MPI 355 Polymer Research, Wiley Online Library on [24/04/2024]. See the Terms and Conditions (https://onlinelibrary.wiley.com/terms-and-conditions) on Wiley Online Library for rules of use; OA articles are governed by the applicable Creative Commons License

ure S22). Additionally, in situ ESR) spectroscopy was used to distinguish between the types of free radicals present. Notably, the presence of a distinct six-fold signal peak in the ESR spectrum was attributed to the benzyl radical generated by the interaction of toluene with CTF-Th-0 during the photocatalytic process (Figure 2d).

DFT calculations provided insights into the reaction energetics of each step in the selective photocatalytic oxidation of toluene. The calculated Gibbs free energies (ΔG) for each reaction are shown in Figure 2e, with the adsorption of toluene molecules on the surface of the CTFs being energetically favorable. CTF-Th-0 exhibited a higher ΔG for toluene adsorption (−0.34 eV) than CTF-Th-1 (−0.25 eV) and CTF-Th-2 (−0.20 eV), indicating stronger toluene adsorption capability. The rate-limiting step was the formation of a benzyl radical ($^*C_7H_8 + h^+ \rightarrow {}^*C_7H_7^{\bullet} + H^+$). Importantly, CTF-Th-0 (2.01 eV) exhibited a significantly lower reaction energy for the alkylbenzylic radical than CTF-Th-1 (2.48 eV) and CTF-Th-2 (2.72 eV), indicating its more efficient promotion of the photocatalytic selective oxidation of toluene. This result suggests that CTF-Th-0 can accelerate the selective photocatalytic oxidation of toluene because of the significant modulation effects of the spacer, which enhances the generation of photogenerated holes at the active oxidation sites, promotes carrier transfer, and optimizes the surface activation mode. Overall, these DFT calculations support the experimental results and provide a molecular-level understanding of the CFT photocatalytic properties.

Based on the above observations and previous report,[17] a reaction mechanism is proposed (Figure 2f). Under visible-light irradiation, the excited photocatalyst activates oxygen on its surface to generate $^1O_2$ and $O_2^{\bullet-}$ through single-electron and energy transfer. Subsequently, the positive holes oxidize the C(sp^3)–H bond of toluene to the corresponding benzylic radical, which undergoes proton abstraction. The reaction intermediate then reacts with $^1O_2$ and $O2^{\bullet-}$ to form alkylperoxyl radicals and alkylperoxides, respectively, which are further decomposed to obtain the final product benzaldehyde.

To explore the origin of the superior activity and selectivity for the oxidation of toluene over CTF-Th-0, the charge excitation and separation performances were investigated. CTF-Th-0 exhibited the highest photocurrent intensity (Figure S23a), indicating its high conductivity and light-induced charge mobility within the polymer. In the EIS spectra (Figure S23b), all polymers show semicircular plots which can be fitted by a Randles equivalent circuit (inset in Figure S23b), where R_{es}, R_{ct} and CPE are the electrolyte solution resistance, charge transfer resistance and constant phase element, respectively.[18] The matching values are given in Table S2. CTF-Th-0 has a R_{ct} of 18.54 kohm, which is the lowest of all the polymers tested. These results support that CTF-Th-0 has the lowest charge transfer resistance, i.e. the fastest charge transfer kinetics. Temperature-dependent photoluminescence (PL) spectra were obtained to elucidate the charge recombination and separation kinetics of the CTFs. The exciton binding energy (E_a) of the PL quenching process was estimated using the Arrhenius equation,[19] and the results showed that CTF-Th-0 had the lowest E_a value (Figure 3a–c), indicating that nonradiative pathways, such as charge separation, occurred more readily in CTF-Th-0. Optical pump THz-probe (OPTP) spectroscopy is a purely optical method that measures the photoconductivity and quantifies the intrinsic charge-carrier mobility of samples in a contact-free fashion.[20] The CTFs exhibited $\varphi\mu$ values (φ

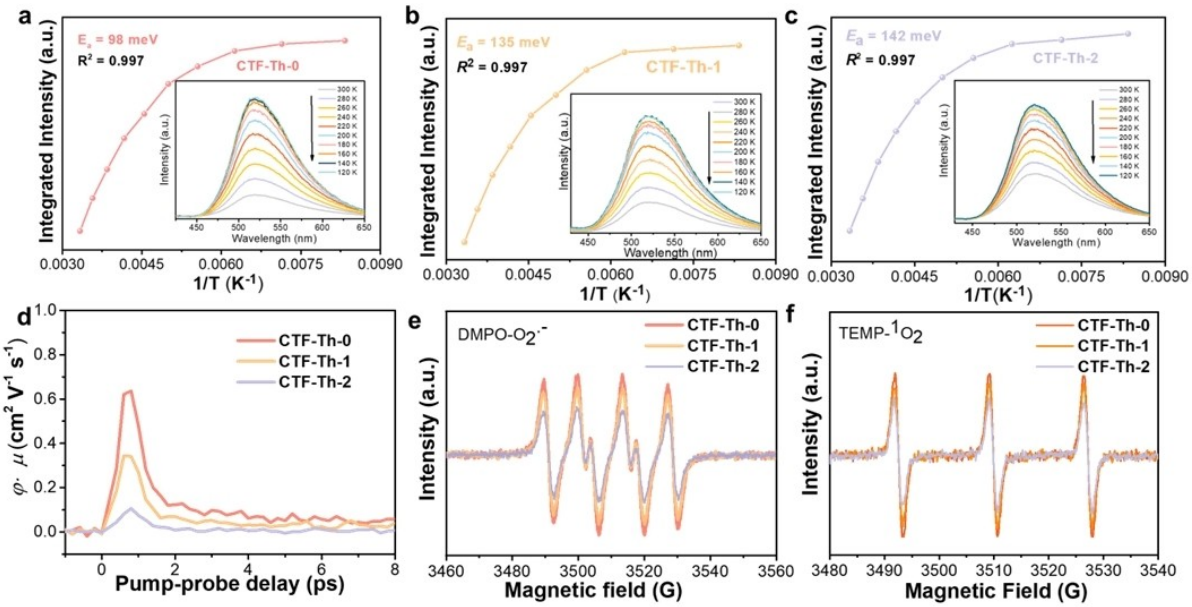

Figure 3. Electrochemical characterization of CTFs. Temperature-dependent PL spectra and corresponding fitting curves (inset) of (a) CTF-Th-0, (b) CTF-Th-1, and (c) CTF-Th-2. (d) THz photoconductivity dynamics of CTFs upon photoexcitation with a 400 nm pulsed laser at an incident photon density of 1×1015 cm^{-2}. ESR spectra of the CTFs in the presence of (e) DMPO and (f) TEMP.

© 2024 The Authors. Angewandte Chemie International Edition published by Wiley-VCH GmbH

15213773, 2024, 18, Downloaded from https://onlinelibrary.wiley.com/doi/10.1002/anie.202400101 by MPI 355 Polymer Research, Wiley Online Library on [24/04/2024]. See the Terms and Conditions (https://onlinelibrary.wiley.com/terms-and-conditions) on Wiley Online Library for rules of use; OA articles are governed by the applicable Creative Commons License

represents the photocarrier generation quantum yield and μ stands for the charge carrier mobility) ranging from 0.1 to 0.6 $cm^2 V^{-1} s^{-1}$, with CTF-Th-0 showing the highest $\varphi\mu$ value (Figure 3d), indicating high charge-carrier mobility that enables the effective transport of photogenerated carriers between donor and acceptor units in CTF-Th-0, thus promoting the photoinduced generation of holes at the active oxidation sites. Moreover, room-temperature PL spectra (Figure S24) were recorded, and the results showed that CTF-Th-0 had a significantly lower PL intensity than the other CTFs, suggesting that the lower number of phenylene spacer units in CTF-Th-0 promoted charge separation. These results suggest that CTF-Th-0 has better charge transport properties and charge separation efficiency than the other CTFs, which contributes to its superior photocatalytic activity and selectivity for toluene oxidation. The ESR technique was used to confirm the formation of reactive oxygen species such as $O_2^{\bullet-}$ and $^1O_2$ in the catalytic process of selective oxidation reactions. Two trapping agents, 5,5-dimethyl-1-pyrroline N-oxide (DMPO) and 2,2,6,6-tetramethylpiperidine (TEMP), were used to capture the species. The ESR intensity of CTF-Th-0 was found to be the highest among the CTFs under visible-light irradiation, indicating its optimal activity (Figure 3e and 3f).

To further monitor the electron-hole separation and elucidate the efficient charge transfer of the CTFs, fs-TA measurements were performed under 400 nm excitation to track the real-time photogenerated carrier dynamics. As illustrated in Figure 4a–c, a broad negative absorption band was observed for all CTFs, mainly due to stimulated emission and state filling of photobleaching. In the region between 530 and 580 nm, a negative peak corresponding to the signal of the photoexcited holes was observed. CTF-Th-0 showed the strongest negative signal compared to those of the other CTFs, suggesting that it produced the most photogenerated holes.[21] To estimate the decay kinetics of photogenerated carrier in the CTFs, the time distribution of TAS probed at 540 nm were fitted by a three-exponential function. The τ1 corresponded to the process of shallow electron capture by hole, and long life τ2 was due to the interface carrier transferred process, τ3 could be attributed to the recombination of holes, and impurity electrons.[22] As shown in Figure 4d–f, the decay lifetimes for CTF-Th-0 were τ1 = 14.2 ps, τ2 = 876.5 ps, and τ3 = 1581.6 ps. Analogously, CTF-Th-1 exhibited comparable results of τ1 = 8.5 ps, τ2 = 538.3 ps, and τ3 = 927.1 ps, while CTF-Th-2 showcased analogous outcomes of τ1 = 3.3 ps, τ2 = 335.6 ps, and τ3 = 653.8 ps. Compared with the other two samples, the longer t1 and t2 decays indicate that the photogenerated holes in CTF-Th-0 are present for a longer period of time, effectively delaying the electron-hole complexation, whereas t3 suggests that the carrier lifetimes in CTF-Th-0 have been greatly prolonged, enhancing the photocatalytic performance.[23]

Generally, the direct activation of saturated sp^3 C–H bonds is initiated by photoactivated holes with sufficient oxidizing ability. The in situ XPS measurements of CTF-Th-0 provided insights into the generation of holes in the CTFs (Figure 5a–c). The binding energy changes of various elements in the presence or absence of light were analyzed. An increase in the binding energy suggests a decrease in the electron cloud density, indicating that electron transfer occurred at the corresponding atoms. Under visible-light irradiation, the binding energy of the S 2p peak shifted toward a higher energy compared to that in the dark, indicating that the S atoms partially transferred electrons to

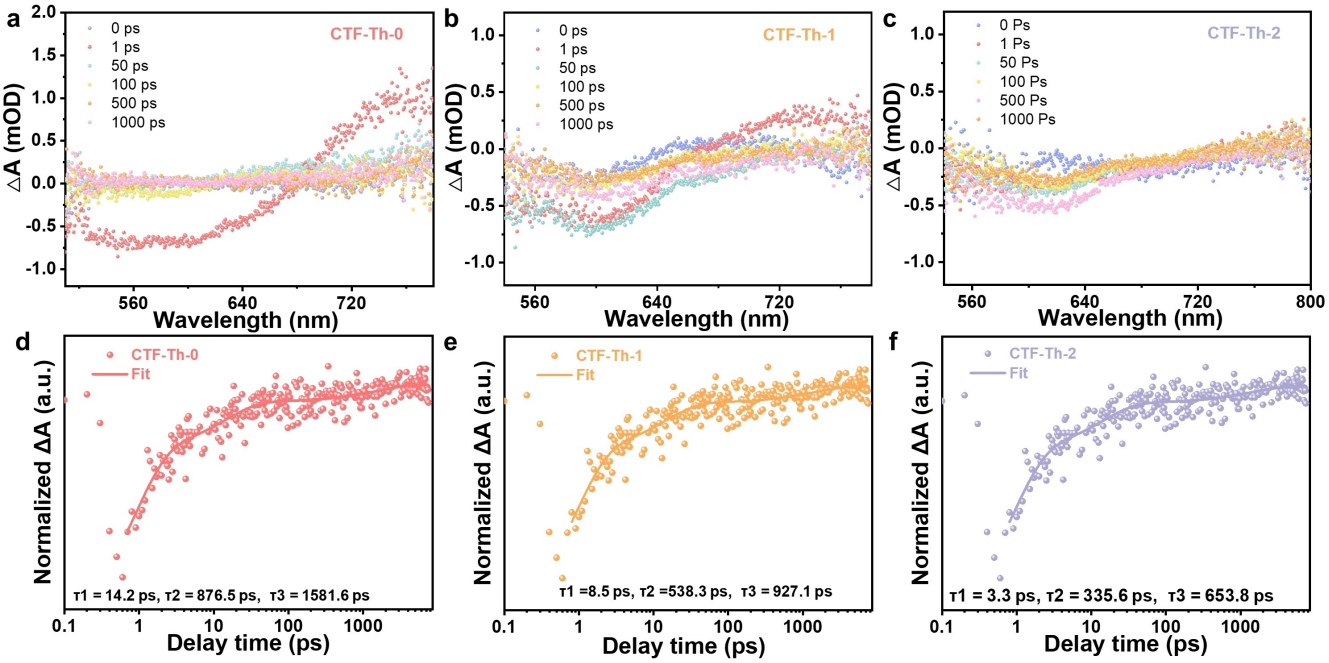

Figure 4. The dynamics of photoinduced charge carriers of CTFs. Transient absorption signals of (a) CTF-Th-0, (b) CTF-Th-1, and (c) CTF-Th-2. The decay signals of (d) CTF-Th-0, (e) CTF-Th-1, and (f) CTF-Th-2.

© 2024 The Authors. Angewandte Chemie International Edition published by Wiley-VCH GmbH

15213773, 2024, 18, Downloaded from https://onlinelibrary.wiley.com/doi/10.1002/anie.202400101 by MPI 355 Polymer Research, Wiley Online Library on [24/04/2024]. See the Terms and Conditions (https://onlinelibrary.wiley.com/terms-and-conditions) on Wiley Online Library for rules of use; OA articles are governed by the applicable Creative Commons License

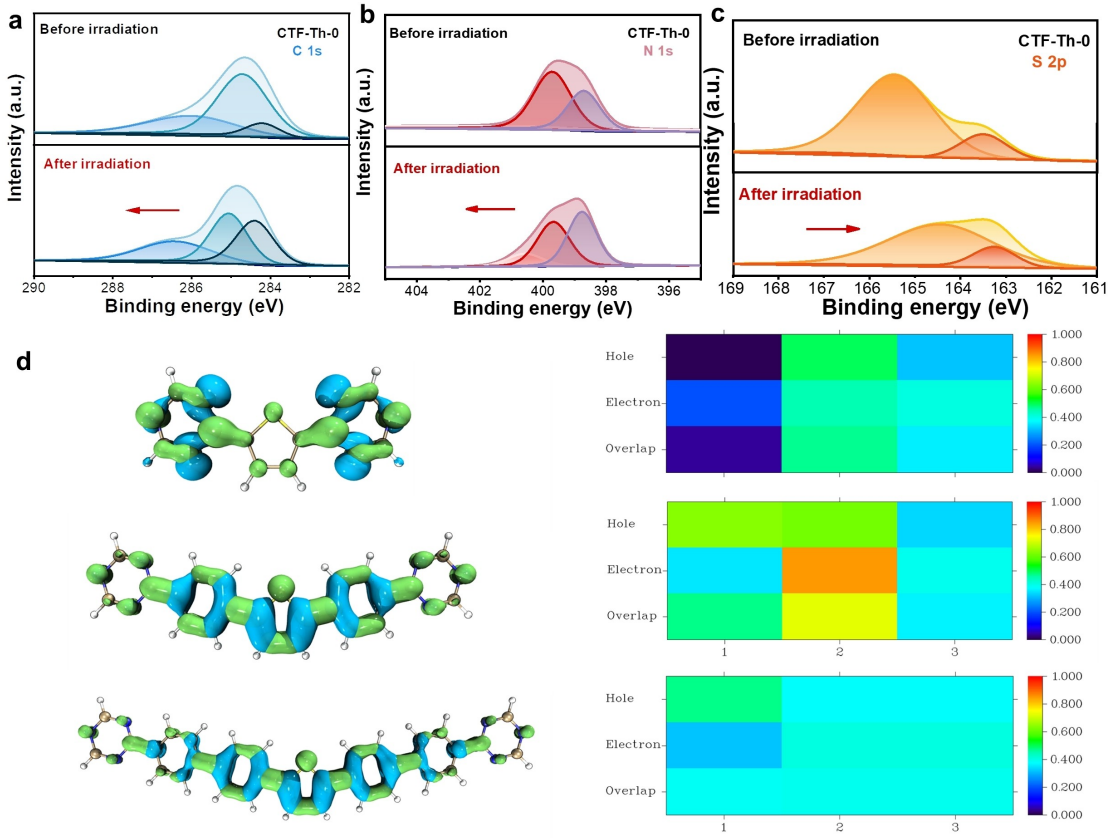

Figure 5. Characterization and DFT calculations of electron transfer in CTFs. In situ XPS spectra of (a) C 1s; (b) N 1s; and (c) S 2p for CTF-Th-0. d, Electron hole distribution of excited monomer fragments (green, electron; blue, hole), and heat map of the electron-hole contribution distribution of excited monomer fragments.

C and N to generate holes. The holes on the S sites then further obtained electrons from the adsorbed toluene, serving as active oxidation sites.[24] TD-DFT calculations were used to investigate the electron and hole distributions in the CTF monomers (Figure 5d).[25] The CTFs were divided into three fragments to study their respective electron and hole contributions. The results showed that the holes were mainly distributed in the thiophene moiety, indicating that the active oxidation active sites were primarily located in this moiety. Moreover, CTF-Th-0 exhibited a higher hole density than the other CTFs, which may explain its superior photocatalytic performance owing to the higher oxidation ability of the polymer.

Conclusion

In summary, we have developed a series of thiophene-based covalent triazine frameworks (CTFs) as effective and robust metal-free heterogeneous photocatalysts operating under visible light for the selective oxidation of sp^3 C–H bonds. Through precise modulation of the phenyl spacer length between the thiophene and triazine units, we have exerted control over the generation of photogenerated holes, consequently influencing the photocatalytic performance. Notably, the heightened concentration of photogenerated holes not only bolstered charge transfer but has also facilitated the cleavage of C(sp^3)–H bonds, a pivotal rate-determining step. In-depth investigations, encompassing in situ XPS measurements and TD-DFT calculations, have conclusively identified the sulfur atoms within the thiophene units as the primary oxidation sites, activated upon the generation of photogenerated holes.

Significantly, the photocatalytic efficacy of CTF-Th-0 has eclipsed the performance of cutting-edge catalysts detailed in existing literature. To elucidate the reaction mechanism further, we have harnessed in situ DRIFTS, in situ ESR, and DFT calculations. Noteworthy is the successful synthesis of a precursor for an active pharmaceutical ingredient, substantiated by recycling trials and solvent-free experiments, thereby underscoring the remarkable applicability of the polymer. Given the myriad structural and synthetic possibilities within the realm of CTF materials, this study not only contributes a fresh perspective to the targeted design of advanced metal-free photocatalysts but also underscores the potential of such materials in fostering innovative strides within the field.

© 2024 The Authors. Angewandte Chemie International Edition published by Wiley-VCH GmbH

15213773, 2024, 18, Downloaded from https://onlinelibrary.wiley.com/doi/10.1002/anie.202400101 by MPI 355 Polymer Research, Wiley Online Library on [24/04/2024]. See the Terms and Conditions (https://onlinelibrary.wiley.com/terms-and-conditions) on Wiley Online Library for rules of use; OA articles are governed by the applicable Creative Commons License

Acknowledgements

The authors acknowledge the National Natural Science Foundation of China (Grants No.: 52173198 and 52303267) and the China Postdoctoral Science Foundation (Certificate No.: 2023M730615) for financial support. We thank R. Graf, M. Steiert, and P. Räder at Max-Planck Institute for Polymer Research for CP-MAS NMR, XRD and TGA measurements. We acknowledge the great help from Dr. H. Wang and Dr. S. Fu at Max-Planck Institute for Polymer Research for helpful optical pump THz-probe spectroscopy measurements and discussion. Open Access funding enabled and organized by Projekt DEAL.

Conflict of Interest

The authors declare no conflict of interest.

Data Availability Statement

The data that support the findings of this study are available from the corresponding author upon reasonable request.

Keywords: covalent triazine framework · photocatalysis · metal-free catalyst · selective oxidation · C–H activation · sp^3 oxidation

[1] a) G. Qi, T. E. Davies, A. Nasrallah, M. A. Sainna, A. G. R. Howe, R. J. Lewis, M. Quesne, C. R. A. Catlow, D. J. Willock, Q. He, D. Bethell, M. J. Howard, B. A. Murrer, B. Harrison, C. J. Kiely, X. Zhao, F. Deng, J. Xu, G. J. Hutchings, *Nature Catalysis* **2022**, *5*, 45–54; b) H. Sterckx, B. Morel, B. U. W. Maes, *Angew. Chem. Int. Ed.* **2019**, *58*, 7946–7970; c) Z. Chen, M.-Y. Rong, J. Nie, X.-F. Zhu, B.-F. Shi, J.-A. Ma, *Chem. Soc. Rev.* **2019**, *48*, 4921–4942.

[2] a) A. K. Cook, S. D. Schimler, A. J. Matzger, M. S. Sanford, *Science* **2016**, *351*, 1421–1424; b) L. Kesavan, R. Tiruvalam, M. H. A. Rahim, M. I. bin Saiman, D. I. Enache, R. L. Jenkins, N. Dimitratos, J. A. Lopez-Sanchez, S. H. Taylor, D. W. Knight, C. J. Kiely, G. J. Hutchings, *Science* **2011**, *331*, 195–199; c) J. Vercammen, M. Bocus, S. Neale, A. Bugaev, P. Tomkins, J. Hajek, S. Van Minnebruggen, A. Soldatov, A. Krajnc, G. Mali, V. Van Speybroeck, D. E. De Vos, *Nature Catalysis* **2020**, *3*, 1002–1009.

[3] a) Z.-J. Bai, S. Tian, T.-Q. Zeng, L. Chen, B.-H. Wang, B. Hu, X. Wang, W. Zhou, J.-B. Pan, S. Shen, J.-K. Guo, T.-L. Xie, Y.-J. Li, C.-T. Au, S.-F. Yin, *ACS Catal.* **2022**, *12*, 15157–15167; b) Y.-X. Tan, Z.-M. Chai, B.-H. Wang, S. Tian, X.-X. Deng, Z.-J. Bai, L. Chen, S. Shen, J.-K. Guo, M.-Q. Cai, C.-T. Au, S.-F. Yin, *ACS Catal.* **2021**, *11*, 2492–2503; c) X. Cao, Z. Chen, R. Lin, W.-C. Cheong, S. Liu, J. Zhang, Q. Peng, C. Chen, T. Han, X. Tong, Y. Wang, R. Shen, W. Zhu, D. Wang, Y. Li, *Nature Catalysis* **2018**, *1*, 704–710; d) Z. Zhang, Y. Yang, Y. Wang, L. Yang, Q. Li, L. Chen, D. Xu, *Angew. Chem. Int. Ed.* **2020**, *59*, 18136–18139.

[4] a) S.-S. Zhu, Y. Liu, X.-L. Chen, L.-B. Qu, B. Yu, *ACS Catal.* **2022**, *12*, 126–134; b) Q. Zhang, B. An, Y. Lei, Z. Gao, H. Zhang, S. Xue, X. Jin, W. Xu, Z. Wu, M. Wu, X. Yang, W. Wu, *Angew. Chem. Int. Ed.* **2023**, *n/a*, e202304699.

[5] a) X. Li, T. Wang, X. Tao, G. Qiu, C. Li, B. Li, *J. Mater. Chem. A* **2020**, *8*, 17657–17669; b) R. Ghalta, R. Srivastava, *Catalysis Science, Technology* **2023**, *13*, 1541–1557.

[6] a) X. Cao, A. Huang, C. Liang, H.-C. Chen, T. Han, R. Lin, Q. Peng, Z. Zhuang, R. Shen, H. M. Chen, Y. Yu, C. Chen, Y. Li, *J. Am. Chem. Soc.* **2022**, *144*, 3386–3397; b) Q.-Y. Meng, T. E. Schirmer, A. L. Berger, K. Donabauer, B. König, *J. Am. Chem. Soc.* **2019**, *141*, 11393–11397.

[7] Y.-Z. Chen, Z. U. Wang, H. Wang, J. Lu, S.-H. Yu, H.-L. Jiang, *J. Am. Chem. Soc.* **2017**, *139*, 2035–2044.

[8] L. Xiong, J. Tang, *Adv. Energy Mater.* **2021**, *11*, 2003216.

[9] a) M. Yang, R. Lian, X. Zhang, C. Wang, J. Cheng, X. Wang, *Nat. Commun.* **2022**, *13*, 4900; b) T. Yuan, L. Sun, Z. Wu, R. Wang, X. Cai, W. Lin, M. Zheng, X. Wang, *Nature Catalysis* **2022**, *5*, 1157–1168; c) Z. Zhang, J. Jia, Y. Zhi, S. Ma, X. Liu, *Chem. Soc. Rev.* **2022**, *51*, 2444–2490; d) A. López-Magano, S. Daliran, A. R. Oveisi, R. Mas-Ballesté, A. Dhakshinamoorthy, J. Alemán, H. Garcia, R. Luque, *Adv. Mater.* **2023**, *35*, 2209475; e) T. Yuan, Z. Wu, S. Zhai, R. Wang, S. Wu, J. Cheng, M. Zheng, X. Wang, *Angew. Chem. Int. Ed.* **2023**, *62*, e202304861.

[10] a) W. Chen, L. Wang, D. Mo, F. He, Z. Wen, X. Wu, H. Xu, L. Chen, *Angew. Chem. Int. Ed.* **2020**, *59*, 16902–16909; b) D. Chen, W. Chen, Y. Wu, L. Wang, X. Wu, H. Xu, L. Chen, *Angew. Chem. Int. Ed.* **2023**, *62*, e202217479; c) Y. Li, Q. Chen, T. Xu, Z. Xie, J. Liu, X. Yu, S. Ma, T. Qin, L. Chen, *J. Am. Chem. Soc.* **2019**, *141*, 13822–13828.

[11] a) L. Guo, Y. Niu, H. Xu, Q. Li, S. Razzaque, Q. Huang, S. Jin, B. Tan, *J. Mater. Chem. A* **2018**, *6*, 19775–19781; b) M. Liu, K. Yang, Z. Li, E. Fan, H. Fu, L. Zhang, Y. Zhang, Z. Zheng, *Chem. Commun.* **2022**, *58*, 92–95.

[12] a) N. Wang, G. Cheng, L. Guo, B. Tan, S. Jin, *Adv. Funct. Mater.* **2019**, *29*, 1904781; b) W. Huang, N. Huber, S. Jiang, K. Landfester, K. A. I. Zhang, *Angew. Chem. Int. Ed.* **2020**, *59*, 18368–18373; c) H. S. Sasmal, A. Kumar Mahato, P. Majumder, R. Banerjee, *J. Am. Chem. Soc.* **2022**, *144*, 11482–11498.

[13] a) X. Wang, L. Chen, S. Y. Chong, M. A. Little, Y. Wu, W.-H. Zhu, R. Clowes, Y. Yan, M. A. Zwijnenburg, R. S. Sprick, A. I. Cooper, *Nat. Chem.* **2018**, *10*, 1180–1189; b) W. Zhao, P. Yan, B. Li, M. Bahri, L. Liu, X. Zhou, R. Clowes, N. D. Browning, Y. Wu, J. W. Ward, A. I. Cooper, *J. Am. Chem. Soc.* **2022**, *144*, 9902–9909; c) T. Zhang, G. Zhang, L. Chen, *Acc. Chem. Res.* **2022**, *55*, 795–808.

[14] a) S. Zhang, G. Cheng, L. Guo, N. Wang, B. Tan, S. Jin, *Angew. Chem. Int. Ed.* **2020**, *59*, 6007–6014; b) W. Huang, Q. He, Y. Hu, Y. Li, *Angew. Chem. Int. Ed.* **2019**, *58*, 8944–8944; c) Y. Hu, W. Huang, H. Wang, Q. He, Y. Zhou, P. Yang, Y. Li, Y. Li, *Angew. Chem. Int. Ed.* **2020**, *59*, 14378–14382; d) C. Ayed, J. Yin, K. Landfester, K. A. I. Zhang, *Angew. Chem. Int. Ed.* **2023**, *62*, e202216159.

[15] a) S. Han, Z. Li, S. Ma, Y. Zhi, H. Xia, X. Chen, X. Liu, *J. Mater. Chem. A* **2021**, *9*, 3333–3340; b) W. Zou, Y. Cheng, Y.-X. Ye, X. Wei, Q. Tong, L. Dong, G. Ouyang, *Angew. Chem. Int. Ed.* **2023**, *62*, e202313392; c) X. Ruan, C. Huang, H. Cheng, Z. Zhang, Y. Cui, Z. Li, T. Xie, K. Ba, H. Zhang, L. Zhang, *Adv. Mater.* **2023**, *35*, 2209141.

[16] J. Li, B. Ren, X. Yan, P. Li, S. Gao, R. Cao, *J. Catal.* **2021**, *395*, 227–235.

[17] a) C. Xu, Y. Pan, G. Wan, H. Liu, L. Wang, H. Zhou, S.-H. Yu, H.-L. Jiang, *J. Am. Chem. Soc.* **2019**, *141*, 19110–19117; b) M. Y. Gao, H. Bai, X. Cui, S. Liu, S. Ling, T. Kong, B. Bai, C. Hu, Y. Dai, Y. Zhao, *Angew. Chem.* **2022**, *134*, e202215540.

[18] S. Wang, X. Wu, J. Fang, F. Zhang, Y. Liu, H. Liu, Y. He, M. Luo, R. Li, *ACS Catal.* **2023**, *13*, 4433–4443.

[19] Z.-A. Lan, G. Zhang, X. Chen, Y. Zhang, K. A. I. Zhang, X. Wang, *Angew. Chem. Int. Ed.* **2019**, *58*, 10236–10240.

© 2024 The Authors. Angewandte Chemie International Edition published by Wiley-VCH GmbH

15213773, 2024, 18, Downloaded from https://onlinelibrary.wiley.com/doi/10.1002/anie.202400101 by MPI 355 Polymer Research, Wiley Online Library on [24/04/2024]. See the Terms and Conditions (https://onlinelibrary.wiley.com/terms-and-conditions) on Wiley Online Library for rules of use; OA articles are governed by the applicable Creative Commons License

[20] S. Fu, E. Jin, H. Hanayama, W. Zheng, H. Zhang, L. Di Virgilio, M. A. Addicoat, M. Mezger, A. Narita, M. Bonn, K. Müllen, H. I. Wang, *J. Am. Chem. Soc.* **2022**, *144*, 7489–7496.
[21] H. Ou, S. Ning, P. Zhu, S. Chen, A. Han, Q. Kang, Z. Hu, J. Ye, D. Wang, Y. Li, *Angew. Chem. Int. Ed.* **2022**, *61*, e202206579.
[22] a) F. Liu, R. Shi, Z. Wang, Y. Weng, C. M. Che, Y. Chen, *Angew. Chem.* **2019**, *131*, 11917–11921; b) A. Wang, M. Du, J. Ni, D. Liu, Y. Pan, X. Liang, D. Liu, J. Ma, J. Wang, W. Wang, *Nat. Commun.* **2023**, *14*, 6733.
[23] a) C. Ye, J.-X. Li, Z.-J. Li, X.-B. Li, X.-B. Fan, L.-P. Zhang, B. Chen, C.-H. Tung, L.-Z. Wu, *ACS Catal.* **2015**, *5*, 6973–6979; b) R. Gao, J. Bai, R. Shen, L. Hao, C. Huang, L. Wang, G. Liang, P. Zhang, X. Li, *J. Mater. Sci. Technol.* **2023**, *137*, 223–231; c) C. Bie, B. Zhu, L. Wang, H. Yu, C. Jiang, T. Chen, J. Yu, *Angew. Chem. Int. Ed.* **2022**, *61*, e202212045.
[24] C. Cheng, J. Zhang, B. Zhu, G. Liang, L. Zhang, J. Yu, *Angew. Chem. Int. Ed.* **2023**, *62*, e202218688.
[25] T. Lu, F. Chen, *J. Comput. Chem.* **2012**, *33*, 580–592.

Manuscript received: January 2, 2024
Accepted manuscript online: February 26, 2024
Version of record online: March 27, 2024

© 2024 The Authors. Angewandte Chemie International Edition published by Wiley-VCH GmbH

15213773, 2024, 18, Downloaded from https://onlinelibrary.wiley.com/doi/10.1002/anie.202400101 by MPI 355 Polymer Research, Wiley Online Library on [24/04/2024]. See the Terms and Conditions (https://onlinelibrary.wiley.com/terms-and-conditions) on Wiley Online Library for rules of use; OA articles are governed by the applicable Creative Commons License